Development of a Dual Function Joint Modular Soft Actuator and its Evaluation using a Novel Dummy Finger Joint-Soft Actuator Complex Model

Pablo E. Tortós-Vinocour[1], Shota Kokubu[1], Fuko Matsunaga[1], Yuxi Lu[1], Zhongchao Zhou[1], Jose Gomez-Tames[2], *Member, IEEE* and Wenwei Yu[3] *Member, IEEE*

***Abstract*— Soft actuators, made from soft materials, offer a safer alternative to rigid robots for use on hand rehabilitation devices. A current challenge is to ensure these actuators comply with human finger morphology. To gain better insights into actuator mechanics when worn on and interacting with human fingers, combining physical experiments with simulation approaches is necessary. However, no simulation has been implemented for finger-actuator interactions. This study proposes a new joint modular soft actuator designed to comply with a dummy finger joint. The new actuator has a dual function design for increasing axial elongation during bending, facilitating compliance with finger morphology. In addition, a novel FEM for the new actuator's interaction with the dummy finger joint (dummy joint-soft actuator complex) is developed and used with physical experiments for evaluating actuator performance. Results show that the new design increases the dummy joint's bending range while exerting smaller contact forces on the joint. Even when the joint is blocked at specific bending angles, the actuator remains compliant to finger morphology. This research is a significant advancement in soft actuator design for hand rehabilitation, emphasizing the interaction between human fingers and soft actuators.**

***Index Terms*—Soft Robots Materials and Design, Modeling, Control and Learning for Soft Robots, Rehabilitation Robotics**

Manuscript received: November 2, 2023; Revised February 2, 2024; Accepted February 22, 2024.

This paper was recommended for publication by Editor Pietro Valdastri upon evaluation of the Associate Editor and Reviewers' comments. This work was supported by a Grant-in-Aid for Scientific Research under Grant KAKENHI JP22H03450 from MEXT/JSPS and by the Japanese Ministry of Education, Culture, Sports, Science, and Technology through the MEXT Scholarship for Research Students (Scholarship No.200417). *(Corresponding author: Jose Gomez-Tames)*

[1]Pablo E. Tortos Vinocour, Shota Kokubu, Fuko Matsunaga, Yuxi Lu, Zhongchao Zhou are with the Graduate School of Science and Engineering, Chiba University, Chiba 2638522, Japan. (ccta0833@chiba-u.jp, s.kokubu@chiba-u.jp, matsunagafuko@chiba-u.jp, yuxi.lu@chiba-u.jp, zhouzhongchao@outlook.com).

[2]Jose Gomez-Tames is with the Graduate School of Science and Engineering, Chiba University, Chiba 2638522, Japan, and also with the Center for Frontier Medical Engineering, Chiba University, Chiba 2638522, Japan (e-mail: jgomez@chiba-u.jp, tel: +81-43-290-3499)

[3]Wenwei Yu is with the Graduate School of Science and Engineering, Chiba University, Chiba 2638522, Japan, and also with the Center for Frontier Medical Engineering, Chiba University, Chiba 2638522, Japan (yuwill@faculty.chiba-u.jp)

Digital Object Identifier (DOI): see top of this page

I. Introduction

THE ongoing aging of the population has led to an increase in stroke patients worldwide [1]. Around 42.6% of stroke survivors can present hand mobility problems and therefore require permanent or temporal hand rehabilitation [2]. The use of soft robotic hand rehabilitation devices has risen as an alternative for motion assistance and rehabilitation in these patients [3].

Soft actuators used in hand rehabilitation have usually been designed to actuate on a whole finger by simultaneously mobilizing all finger joints together (hereafter, whole-finger type actuators) [4]. This type of actuator, however, ignores the individual patient's finger dimensions and finger joint position, which can reduce the effectiveness of rehabilitation [5],[6].

Multipocket soft actuators have been proposed to adapt to different finger dimensions by having individual air chambers for each finger joint [5]. However, these soft actuators present problems with the force transmitted from the actuator to the finger due to the energy lost from the deformation of the silicon between chambers [6]. Modular joint soft actuators have been proposed as a solution to the aforementioned problems so that each actuator can independently actuate on each finger joint.

When worn on human fingers, the behavior of the soft actuators can change due to the friction between the actuator and the finger, as well as the resistance to passive movement exerted by finger joints. To investigate the interaction between fingers and soft actuators, several studies [5],[6],[7] have incorporated the use of dummy fingers for evaluating the performance of soft actuators. Performance has been evaluated in terms of bending angle, torque, or force transmission using physical experiments. To the best of our knowledge, the current joint modular soft actuators have not considered the interaction between the soft actuators and the fingers in their actuator design [6],[8]. In addition, relying solely on physical experiments is insufficient for evaluating the interaction between soft actuators and human fingers while also prolonging the time required for actuator design optimization.

Finite Element Modeling (FEM) has recently risen as a valuable tool for computational models of soft actuators [9],[10],[11]. However, no FEM has been made to study the interaction between fingers and soft actuators yet. In a previous study, we also constructed an FEM model for controlling air pressure and bending angles in a modular joint soft actuator,

without taking into consideration the interaction with a dummy joint [12]. One challenge when simulating the interaction between fingers and soft actuators is that it involves dealing with multiple soft and rigid bodies, which can be complex as it requires the simulation of friction between contact surfaces. Adequate simulation of the physical constraints between the actuator and the dummy is needed, as well as an accurate representation of the material model of the soft actuator [9]. The objective of this study was to enhance the fitting of a soft actuator to a dummy finger joint by proposing a new modular joint soft actuator design. Specifically, the focus was on designing modular joint soft actuators, considering the interaction between the soft actuator and a dummy finger joint. Previous research has suggested that when a soft actuator cannot comply with a finger's morphology, this can cause the soft actuator to buckle over the finger and affect the actuator's performance [13],[14]. Two previous studies have also shown that incorporating sections dedicated to increasing the axial elongation of a soft actuator makes it possible to increase the actuator's compliance with finger morphology [10],[14]. Both studies, however, only implemented their approach for whole-finger type actuators. In this research, a novel type of pneumatic-driven modular joint soft actuator called the Dual Function Soft Actuator (hereafter, DFSA) was proposed and compared against an Original Modular Actuator (hereafter, OMA) designed in [6]. For the DFSA design, the original design of the OMA is segmented into one section tailored for bending and one section tailored to increase axial elongation, in order to increase the actuator's compliance with finger morphology. Three different types of DFSA with different elongation section lengths were tested and compared with the OMA in terms of bending, both when the actuator is bending independently and when worn on a dummy joint. Both actuators were also compared in terms of the force they generate at the tip of the dummy joint (hereafter, Blocked Joint Tip Force) when the joint is blocked at different angles along its bending trajectory. To the best of our knowledge, previous studies have only shown the compliance of their designs empirically and have not been able to quantify it. A novel FEM was developed for when each actuator type (OMA or DFSA) is attached to a dummy joint (DJ), which we referred to as the dummy joint-soft actuator complex (hereafter, DJ-SA Complex). Previous results have shown that when actuators worn over joints are misaligned with respect to the center of the joint it can lead to significant losses in their bending output [15]. In multiple joint systems, this can happen because of one actuator displacing another one during bending. As it will be shown in this study, displacement can happen due to the actuator not complying with finger morphology, which can cause one end of the actuator to slide in direction towards the joint (hereafter, tip displacement). Using the FEM, we were able to measure tip displacement and used it to quantify the compliance of all designs in all experiments. With the FEM, we calculated the contact forces that the soft actuator applied to the DJ for all the tests done. The structure of the paper is organized as follows: Section 2 provides detailed descriptions of the OMA and DFSA, the DJ, and the DJ-SA complex. Sections 3 and 4 detail the implementation of the FEM for the DFSA, the experimental setup, and the corresponding results. The paper culminates with Sections 5 and 6, where the discussion and conclusion of the study are presented.

II. Design of Modular Actuators and Dummy Joint

A. Original Modular Soft Actuator and Dual Function Soft Actuator Design

In Fig. 1(a), the OMA [6] is illustrated. The dimensions were based on the original results from [6] but increasing the fiber interval from 2 mm to 3 mm to optimize computational resources. The actuator was fabricated from Dragon Skin 10 (Smooth-On, Inc.). It has a Kevlar (Dupont, Inc.) fiber reinforcement, arranged in a two-way hitching layout [5]. Design parameters are *W* (wall thickness) = 1.5 mm, *INT* (fiber interval, adjusted to 3 mm) = 3 mm, *CH* (chamber height) = 7.5 mm, *CL* (chamber length) = 20 mm, and *L* (actuator length) = 23 mm. Fig. 1(b) shows the DFSA with two sections. One is tailored for an axial elongation section, positioned over the DJ's proximal phalanx, using a single-loop fiber wrapping method [9]. Another one is a bending section that has the same fiber wrapping method as the OMA.

Three different types of DFSA with varying elongation

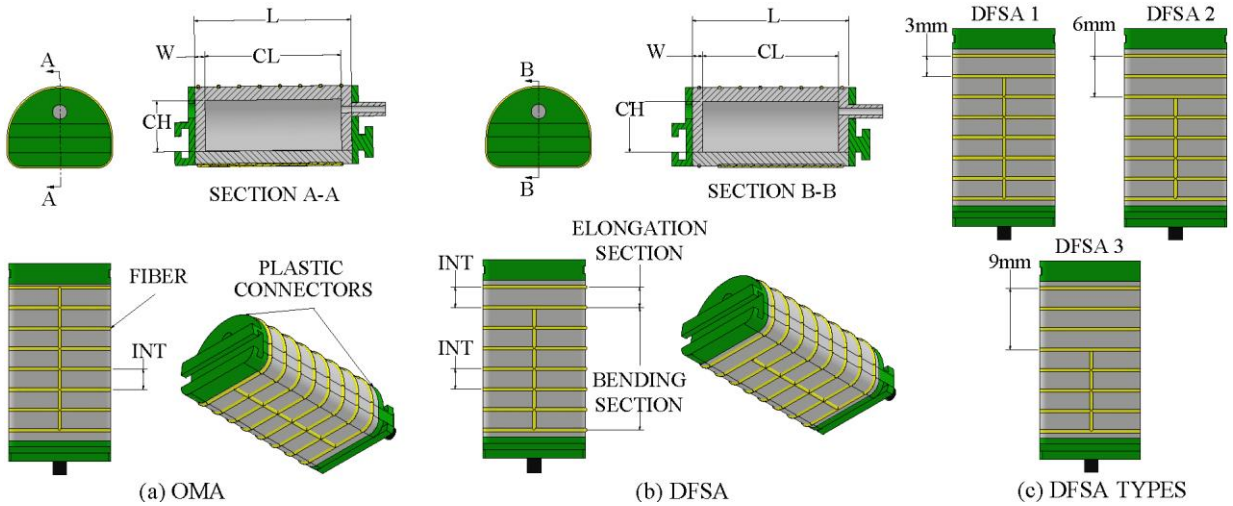

Fig. 1. (a) Design of the OMA. (b) Design of the DFSA. (c) DFSA types with different elongation lengths (DFSA 1, DFSA 2, and DFSA 3).

section lengths were tested (Fig. 1(c)). The lengths for the elongation section were based on the area in contact with the proximal phalanx of the OMA when positioned over the DJ-SA Complex, which was approximately 9 mm long. This 9 mm length was then divided for the three DFSA.

B. Design of the Dummy Joint (DJ)

The DJ used in this design is composed of the sections that correspond with the metacarpal bone, the metacarpophalangeal joint, and the proximal phalanx sections of the dummy finger used for [5] and [6]. The design of the DJ is shown in Fig. 2(a). The dimensions of L_{MP} = 42.34 mm and L_{PP} = 37.95 mm are based on the average dimensions of Japanese index fingers [16]. The entire dummy is made of PLA printed at 20% density. A torsion spring is fixated at the joint axis to represent the joint's resistance to passive movement. A spring with a constant of 0.29 N/deg was selected based on [6]. A coupling link is attached at the end of the actuator (Fig. 2(b)).

C. Coupling of the DJ-SA Complex

Soft actuators are frequently worn on dummy fingers using velcro bands [5],[6]. Simulating these bands can introduce inaccuracies to the model, as the tightness of each band can vary from test to test and can be difficult to represent in simulations. For this reason, in this study, we opted to use an elastic band designed specifically for this experiment (see Fig. 2(c)). Fig. 2(d) shows the position of the proximal phalanx, metacarpal bone, and MCP on the human finger. The elastic band allowed the actuator to slide in the direction parallel to the finger while limiting displacement in the normal direction. The elastic band is made of Smooth-On Sil 950 (Smooth-On, Inc). This material was chosen due to its high young modulus (E = 0.34 MPa [10]) to increase how tight the actuator is held to the dummy and reduce the actuator's buckling. A plastic adapter and two screws are used to fixate the position of the actuator over the DJ. Table I shows a list of the parts and materials of the DJ-SA Complex

TABLE I
LIST OF MATERIALS

Part(s)	Material
Actuator's Body	DragonSkin 10
Fiber Reinforcement	Kevlar
Elastic Band	Smooth-On Sil 950
DJ, Coupling Link, Plastic Connectors, Adapter	PLA

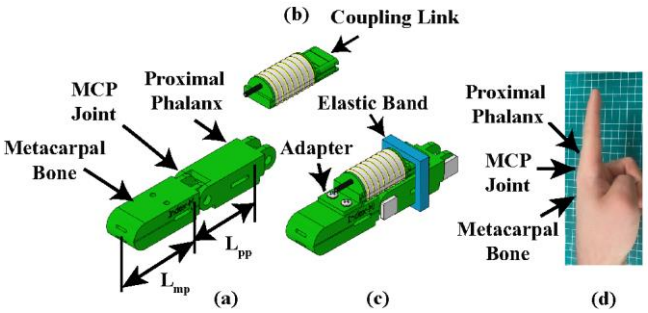

Fig. 2. (a) Soft Actuator with the coupling link attached. (b) Dummy Joint (DJ). (c) DJ-SA Complex (d) Diagram of the MCP joint in a finger.

III. EXPERIMENTAL SETUP AND FEM

A. Bending Angle and Blocked Joint Tip Force Experiments

The actuator is hung from a clamp by attaching a coupling block to the base of the actuator. Augmented Reality (AR) markers are attached to both extremes of the actuator to measure the bending angle (θ). Fig. 3(b) illustrates the bending angle measurement for the DJ-SA Complex. The dummy is also held upside down, and AR markers are attached at the base and the proximal phalanx section of the DJ. Fig. 3(c) shows the experimental setup used for the Blocked Joint Tip Force measurements. The Blocked Joint Tip Force is measured when the DJ-SA Complex is blocked on different bending angles (θ_b) using a load cell (see Fig. 3(c)). For this, the load cell is held static with a clamp and the DJ-SA Complex is rotated along an axis placed in the middle of the joint before initiating the experiment. The force measurements are performed for θ_b = 0°, θ_b = 15°, and θ_b = 30°. For θ_b = 15° and θ_b = 30° conditions, the DJ-SA Complex is first bent freely before impacting the load cell and reaching the blocked position (the joint cannot bend anymore). This set of θ_b values was chosen based on the bending angles achieved by the DJ-SA Complex for both actuators during the bending experiment (see Section 4.A). All actuators had a maximum bending angle of around 40° on the DJ-SA Complex. Values higher than θ_b = 30° were not evaluated as these were too close to the maximum bending angle of the FEM and would only have allowed to record a small amount of measurements. All experiments and models were run to a maximum air pressure of 100 kPa. Two different samples of each actuator type were tested three times each for all experiments and the average values were reported.

B. Finite Element Modeling of the DJ-SA Complex

1) Simulated Scenarios: Three simulation scenarios were implemented to match the physical experiments: the Free Bending Model (Fig. 3(d)), the DJ-SA Complex Bending Model (Fig. 3(e)), and the Blocked Joint Tip Force Measurement Model (Fig. 3(f)).

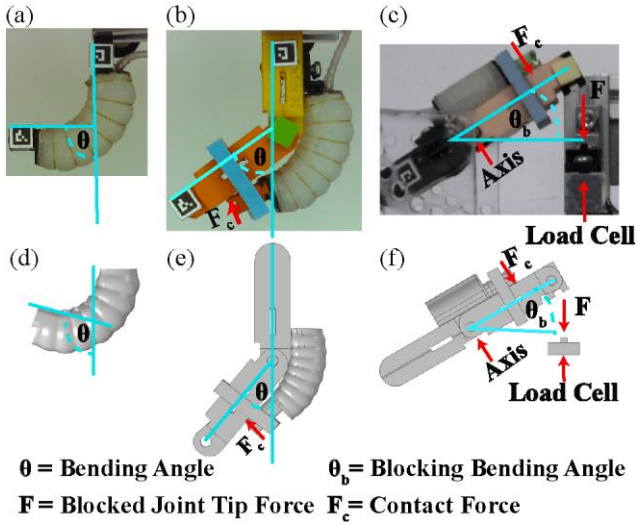

Fig. 3. (a) Free Bending Experiment. (b) DJ-SA Complex Bending Experiment. (c) Blocked Joint Tip Force Measurement Experiment.(d) Free Bending Model. (e) DJ-SA Complex Bending Model. (f) Blocked Joint Tip Force Model.

2) Implementation of the Actuator Models: The Solid Mechanics Interface of the Structural Mechanics Module of COMSOL Multiphysics 5.6® was used to model the soft actuators. Boundary Load conditions are used to simulate the input air pressure. The fiber reinforcement is modeled based on [17] using a square cross-sectional area for reducing computational costs and placed inside the actuator to avoid needing contact conditions between the fibers and the actuator.

3) DJ-SA Complex Implementations: The DJ is modeled using the Solid Mechanics Interface and a hinge joint condition is applied using the Multibody Dynamics Module of COMSOL Multiphysics 5.6®. A spring constraint is applied to the hinge joint to simulate the torsion spring placed at the joint. The elastic band and the coupling link are also modeled using the Solid Mechanics Interface.

4) Meshing and Other Settings: Symmetry was used to reduce computational resources. Based on [18], a mesh made of tetrahedral elements using the default fine mesh setting was used for all components. Boundary meshes were used for mesh refinement in all contact surfaces [17]. These settings were enough to provide numerical convergence without drastically increasing computational resources The number of tetrahedral elements varied among models (minimum of 36,546 for the Free Bending Model with DFSA and maximum of 97,603 for the Blocked Joint Tip Force Measurement Model with DFSA).

5) Material Settings: For the actuators, the Kevlar Fiber Reinforcement was modeled as a Linear Elastic Material with E = 31,670 MPa, ν = 0.36, and ρ = 1,440 kg/m^3 [10], where E, ν, and ρ are the Young Modulus, Poisson's Ratio, and density, respectively. The material PLA for the plastic parts of the actuator and the DJ was also modeled as a linear elastic material with E = 3.5 GPa, ν = 0.36, and ρ = 1,240 kg/m^3 [19]. Both Smooth-On Sil 950 and Dragon Skin 10 were modeled using a Yeoh hyperelastic constitutive model [20]. The engineering Cauchy stress equation for the Yeoh hyperelastic model is presented in (1) where σ and λ are the engineering stress and engineering stretch, respectively. The term I_1 is the first moment of inertia. C_i are known as the Yeoh parameters and n is the order of the model.

$$\sigma=2\left(\lambda-\frac{1}{\lambda^2}\right)\sum_{i=1}^{n} iC_i\left(I_1-3\right)^{i-1} \quad (1)$$

For the Smooth-On Sil 950, an order 1 model was used with C_1 = 0.34 MPa [10], [21]. In the case of DragonSkin10 a Yeoh 3rd order model was used with the parameters calculated from our previous study, C_1 = 0.0477, C_2 = 3.42×10^{-4}, and C_3 = -1.19×10^{-6} [12].

6) Interaction Between Bodies (Contact and Friction): Contact between surfaces was implemented using the default nonlinear penalty contact method from COMSOL Multiphysics 5.6®. Static friction was applied at all contact boundaries in this model. Three different contact interactions were identified. Contact between the soft actuator's body and the dummy finger (contact between PLA and Dragon Skin 10), contact between the coupling link and the elastic band (contact between Smooth-On Sil 950 and PLA), and contact between the coupling link and the dummy finger (contact between PLA and PLA)

7) Coefficient of Friction between PLA and PLA: Several studies have been done previously to measure the coefficient of friction (CoF) of PLA in contact with hard surfaces [19], [22]. In [19] and [22], the CoF of PLA was shown to be dependent on infill density and printing orientation. In [22], PLA parts printed at 20% infill density with a horizontal printing orientation had a CoF between 0.74 and 1.04, depending on the applied load. An intermediate value of 0.89 was assumed in this study to represent the CoF.

8) Coefficient of Friction between PLA and Smooth-On Sil 950 and between PLA and DragonSkin 10: We conducted separate measurements to determine the CoF between PLA and both DragonSkin 10 and Smooth-On Sil 950 (Fig. 4). Tribological measurements were done by Anton Paar Japan, Inc. Measurements were done for 20 different samples of each material. A 4×4 mm^2 PLA plate was used as a static partner and a 20 mm radius disk made of either DragonSkin10 or Smooth-on Sil 950 was used as a counter-solid, depending on the material being tested. The experiments were conducted at a linear speed of 10 mm/s, utilizing both a tribometer and a nanotribometer. The range of tested contact pressures was between 1 and 400 kPa. For the DragonSkin10, however, the PLA plate detached from the experimental platform for a contact pressure of 250 kPa reducing the range of contact pressures measured for this material. The CoF between PLA and both types of silicone varied significantly depending on the contact pressure applied. To capture this variation, the CoF values were represented as mathematical equations derived from logarithmic regressions. Equations (2) and (3) are derived for DragonSkin 10 and Smooth-On Sil 950, respectively.

$$-0.398\ln\left(\text{Contact Pressure}\right)+2.9264 \quad (2)$$

$$-0.014\ln\left(\text{Contact Pressure}\right)+0.7542 \quad (3)$$

When introducing (2) and (3) in the FEM, simulated contact pressures varied from 0 to 62.5 kPa between all models. The R^2, the multiple correlation coefficient (Multiple R), and the p-values are reported and used to evaluate if (2) and (3) fit the experimental data for the previously mentioned ranges of contact pressure (for (3): R^2 = 79.7%, Multiple R = 89.3%, and p-value = 7.56x10^{-22}; for (2): R^2 = 73.7%, Multiple R = 85.9% and p-value = 3.0x10^{-15}). The p-values were both smaller than 0.05 showing that (2) and (3) are statistically significant for the evaluated range of contact pressures. The entire dataset of our experiments is made available online at:

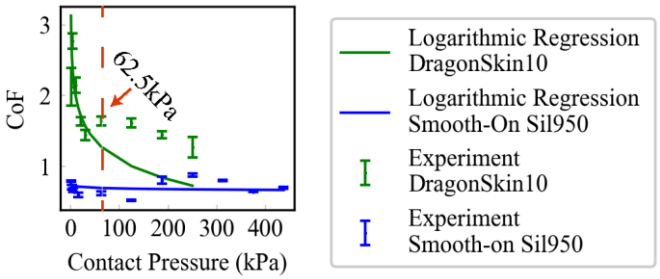

Fig. 4. Experimental Measurements and Logarithmic Regressions of the CoF for DragonSkin 10 and Smooth-on Sil 950 in contact with PLA The red line denotes the limit of the contact pressure range applied on the FEM.

https://github.com/tolstoys19/Friction-Measurements-Between-PLA-and-Silicone

C. Comparison Criteria for the DFSAs and the OMA

Actuator misalignment can lead to up to a 50% loss of total bending angle output [15]. To avoid potential misalignment on other actuators when used for multi-joint systems, we evaluate the actuator tip displacement of DFSA designs (DFSAs 1, 2, and 3) compared to OMA. In addition, the actuators were evaluated in terms of "Contact Force to Bending Angle relationship" for the Bending Angle Experiment (i.e., Contact Force applied from the actuator to the joint vs. Bending Angle) as well as the "Contact Force to Blocked Joint Tip Force relationship" for the Blocked Joint Tip Force Experiment.

IV. Experimental and Simulation Results

A. Effects of Actuator Type on Bending Angle

Fig. 5 displays the bending angle data for both the OMA and the DFSA. In the Free Bending Experiment, the OMA achieved greater bending angles than all the DFSA Actuators in both simulations and physical tests. On the other hand, in the DJ-SA Complex Bending Experiment, the DFSA 1 exhibited the largest bending angles, while DFSA 2 and 3 also outperformed the OMA in both simulated and experimental results. The error between the physical measurements and simulations for both the Free Bending and DJ-SA Complex Bending Experiments was quantified using the mean average error (MAE), root mean square error (RMSE), and the coefficient of determination (R^2), following methodologies from prior studies [11],[23]. For the Free Bending Experiment, the mean values were 4.32° (MAE), 5.82° (RMSE), and 97.17% (R^2). For the DJ-SA Complex Experiment, the mean values were 6.60° (MAE), 7.83 (RMSE), and 97.60% (R^2).

B. Contact Force-Bending Angle Relationship the DJ-SA

The relationship between the contact force and the bending angle for the DJ-SA Complex Bending Experiment (measured on the FEM) is shown in Fig. 6(a). The actuators with the longer elongation section (DFSA 2 and DFSA 3) have the most efficient contact force to bending angle relationship.

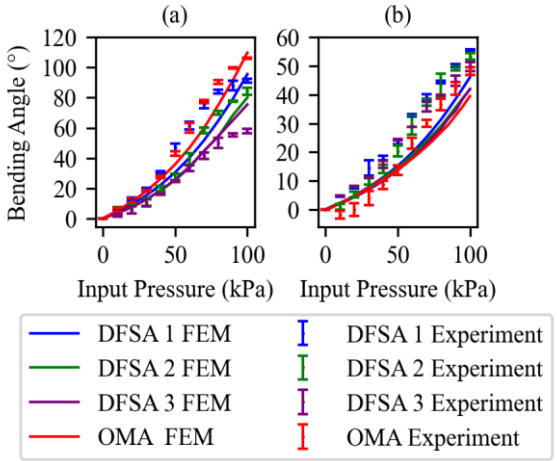

Fig. 5. Experimental and simulation bending results of the OMA and the DFSAs for (a) Free Bending and (b) DJ-SA Complex Experiments.

C. Measurements of Tip Displacement on the Bending Experiment

The relationship between input air pressure and actuator displacement is shown in Fig. 6(a). DFSA 1 has the smallest displacement among all actuator types. This shows that the DFSA 1 has the best compliance with the current DJ size finger morphology. While the OMA didn't have an elongation section, it had significant buckling which caused the tip of the actuator to slide towards the joint.

D. Blocked Joint Tip Force Measurements

Fig. 7 presents both FEM and experimental results for the actuators at three blocking angles θ_b (0°, 15°, and 30°). The average error metrics were calculated for each configuration. For θ_b = 0°: MAE = 0.168 N, RMSE = 0.2, and R^2 = 98.02%. For θ_b = 15°: MAE =0.140 N, RMSE = 0.17, and R^2 = 98.2%. For θ_b = 30°: MAE=0.148 N, RMSE = 0.17, and R^2 = 88.3%. Figs. 3(c) and 3(f) show that the DJ-SA Complex needed to bend to contact the load cell at θ_b = 15° and θ_b = 30°. Physical experiments showed higher bending angles than simulations, leading to earlier contact with the load cell at lower air pressures. This discrepancy was more pronounced at θ_b = 30°, where the experiments made contact at around 60 kPa, and the FEM at 80 kPa. Therefore, the physical experiments recorded higher force values than the FEM at θ_b = 30°, unlike at θ_b = 0° and θ_b = 15°. These results suggest that whereas the OMA applies higher forces for the same air pressure, the DFSA has a more efficient force transmission.

E. Contact Force -Blocked Joint Tip Force Relationship

Figs. 8(a), (b), and (c) show the relationship between the contact force applied from the actuator to the finger and the Blocked Joint Tip Force. Increasing elongation section improved the contact force to bending angle relationship.

F. Tip Displacement on the Blocked Joint Tip Force Experiment

For the blocked joint tip force experiment the total tip displacement from 0 to 100 kPa was measured for all θ_b values for all actuators. The relationship between total tip displacement and input pressure can be seen in Fig. 8(d) Whereas the OMA has smaller values of total tip displacement for θ_b = 0° and θ_b = 15°, the DFSA 1 has the smallest total tip displacement for θ_b= 30°. Furthermore, all the DFSAs have a

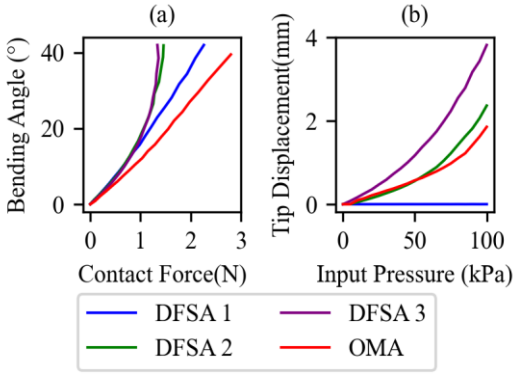

Fig. 6. (a) Relationship between contact force and bending angle (b) Actuator Displacement vs. Input Air Pressure. Both results correspond to FEM simulation in the DJ-SA Complex Bending Experiment.

decreasing tendency on total tip displacement when increasing θ_b whereas the OMA has a U-shape inverted variation of total tip displacement with θ_b.

V. Discussion

This paper proposes a novel modular joint soft actuator called the DFSA, designed to improve compliance with finger morphology by increasing its axial elongation. To evaluate its performance, a FEM of the DJ-SA Complex was developed and employed in conjunction with physical experiments. For this purpose, three different types of DFSA with varying elongation sections were tested. The results from this experiment indicate that all the DFSA types provided a better performance on the DJ-SA Complex when compared to the OMA in terms of (1) higher bending angles and (2) a more efficient force transmission during the Blocked Joint Tip Force Experiments. Furthermore, the DFSA 1 also had a better finger compliance considering a reduced amount of tip displacement when compared to the OMA. The development of the DFSA holds significant potential for impactful advancements in practical applications of soft robotics. The better DFSA's compliance with finger morphology and reduced contact forces can enhance the performance of soft hand rehabilitation devices for long-term users while increasing device safety.

The DFSAs' superior performance in the DJ-SA Complex Bending Experiment is attributed to their more efficient conversion of contact force into bending angle, as shown in simulation results (Fig. 6(a)). This efficiency was related to the increase in axial elongation. DFSA 1 also demonstrated minimal displacement compared to other actuators. Further increases in elongation (DFSA 2 and DFSA 3) led to increased tip displacement, whereas the OMA slid in direction towards the joint due to inadequate compliance with the DJ's bending trajectory which also increased tip displacement. Given the importance of minimizing actuator displacement in multi-joint systems, DFSA 1 was selected as the most effective in the Bending Angle Experiment, due to having minimal tip displacement while still retaining a better "contact force to bending angle relationship" than the OMA. Furthermore, the DFSA 1 had a maximum experimental bending angle of 52° when used on the DJ-SA Complex. This is significantly higher than the values reported at the same air pressure for previous research [7],[8] done under similar conditions (32° and 45° respectively).

During the Blocked Joint Tip Force Experiments, the DFSAs 1 to 3 showed an increased force transmission efficiency, attributed to their axial elongation. This efficient force transmission translates to the DFSAs needing to exert smaller forces on the dummy finger to achieve a desired Blocked Joint Tip Force, thus reducing potential stress on the finger. However, the axial elongation section of the DFSA tends to slide, rather than press, against the finger, limiting its direct force application. On the other hand, the OMA, while not as efficient in force transmission as the DFSAs, generates larger contact forces. As a result, at $\theta_b = 0°$ and $\theta_b = 15°$, the OMA registers higher Blocked Joint Tip Forces than all the DFSAs. This situation changed for $\theta_b = 30°$ due to the OMA's buckling over the DJ, causing significant variation in the angle of

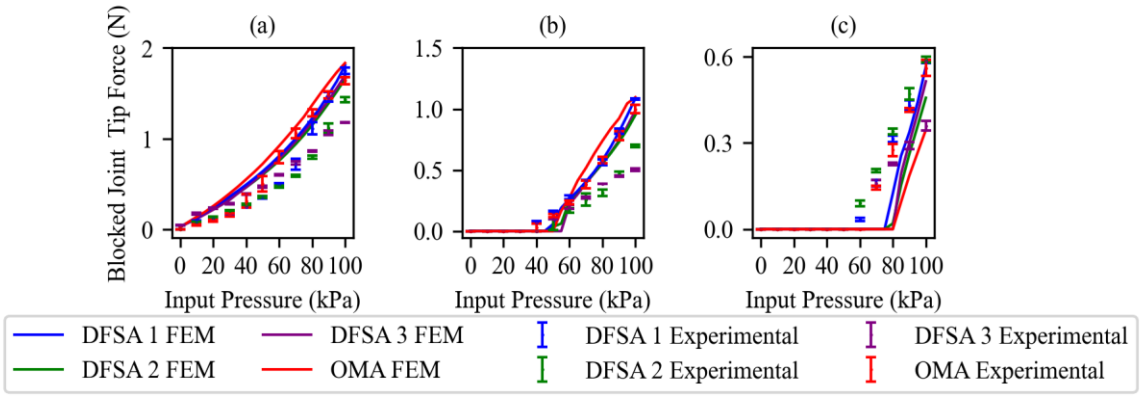

Fig. 7. Experimental and simulation results for the Blocked Joint Tip Force Experiment for the DFSAs and OMA at(a) $\theta_b = 0°$, (b) $\theta_{ib} = 15°$, and (c) $\theta_b = 30°$. Capped vertical lines indicate standard deviation.

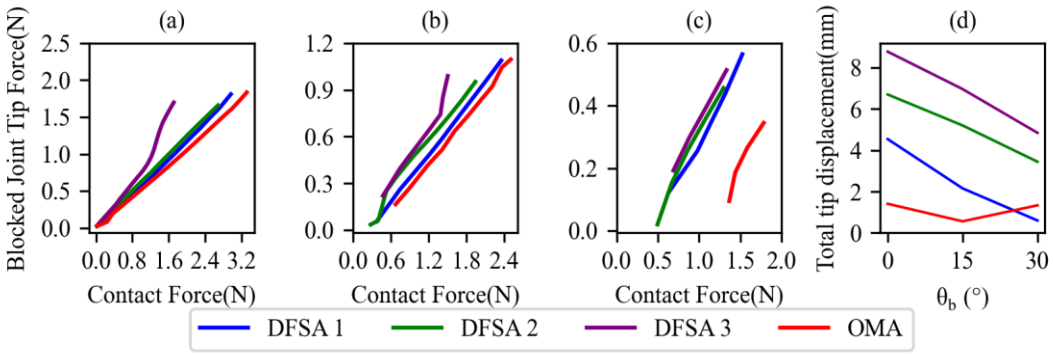

Fig. 8. Contact Force for the Blocked Joint Tip Force Experiment at (a) $\theta_b = 0°$, (b) $\theta_b = 15°$, and (c) $\theta_b = 30°$ based only on FEM stimulation. (d) Total tip displacement for all tested values of θ_b measured on the FEM.

incidence of the contact force (Contact Angle). In Fig. 9 we compared the Contact Angle of the DFSA 1 to the OMA. In here, it can be seen that the OMA has significantly lower contact angles which led to a greater force component applied parallel to the load cell and the DJ, which didn't contribute to the overall Blocked Joint Tip Force output. For the DFSAs total tip displacement tended to decrease when increasing θ_b whereas the OMA's total tip displacement had a U-shape inverted variation with θ_b. This caused that whereas the OMA had smaller values of total tip displacement for θ_b = 0° and θ_b = 15°, the DFSA 1 had the smallest total tip displacement for θ_b = 30°. Further studies should be done to see if the decreasing tendency of the DFSAs remains for higher values of θ_b and for higher air pressure values. Due to the DFSA 1 having the smallest tip displacement while still retaining a better contact force to Blocked Joint Tip Force relationship than the OMA, it was also selected as the most effective in the Blocked Joint Tip Force Experiment. When comparing the total force output of the DFSA 1 it could be seen that the DFSA had a superior performance (1.69 N at 100 kPa) than the results of 0.81 N and 1.32 N reported in two previous studies [5], [6], which were tested under conditions similar to θ_b = 0°. Due to the DFSA 1 also having the best performance in the bending angle experiment, it was then selected as the DFSA actuator with the best performance overall for the current dummy size.

The novel FEM model permitted us to investigate actuators' compliance with finger morphology and bending trajectory, by allowing us to estimate contact forces between the actuator and finger as well as actuator displacement values that are challenging to obtain in physical experiments. Additionally, the FEM allows for the simple insertion of CAD models of different DJs and actuators which can help streamline the testing of different actuator types and different joint sizes. We assessed the accuracy of our FEM models by evaluating three error metrics (MAE, RMSE, R^2) for the Bending Experiments and the Blocked Joint Tip Force Experiment. For the Bending Experiments, the MAE, RMSE, and R^2 values indicated high agreement between physical and simulation results. The R^2 values obtained were close to those reported in previous studies [11], [23], showing the reliability of the FEM. Larger bending angles appeared in physical tests compared to simulations in the DJ-SA Complex Bending Experiment. One reason for the increased angles in physical tests could be the elastic band, which may have exerted a stronger constraint than anticipated. Despite designing the band to match the dimensions of the coupling link and DJ, some tension could be felt in the band when placed over the DJ-SA Complex during physical experiments. This tension may have improved actuator performance by reducing buckling. In the Blocked Joint Tip Force Experiment, the MAE, RMSE, and R^2 values also indicated a general agreement between physical and simulation results. Two among the three tested blocked angle conditions (θ_b = 0° and θ_b = 15°) exhibited R^2 values (98.2% and 98.02% respectively). However, a lower R^2 value (88.3%) was observed for θ_b = 30°. As mentioned in Section 4.D, the physical experiments exhibited higher bending angles than the simulations, which caused an earlier impact on the load cell in the physical experiments. This was more evident in the θ_b = 30° condition, potentially explaining the lower R^2 value.

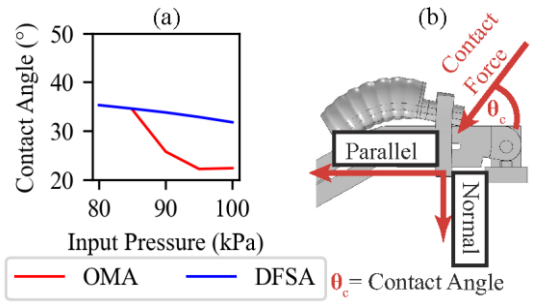

Fig. 9. Contact Angle vs input pressure for the Blocked Joint Tip Force Experiment for the DFSA 1 and the OMA on the FEM.

Additionally, the reference friction values between PLA-PLA surfaces may not have accurately reflected experimental conditions. Furthermore, as mentioned previously in section 3.B.8, friction measurements were done up to a maximum contact pressure of 400 kPa, whereas the FEM reported values up to 62.5 kPa. Taking more measurements between the range of contact pressures applied on the FEM as well as fitting (2) and (3) for these low contact pressures could help increase the accuracy of our models. Measuring the CoF between PLA components should also be considered for this purpose.

Future studies should advance toward the development of complex multi-joint systems and human trials. For that, reducing the computational expensiveness of soft robot models is an important requirement. One approach is adopting a real-time simulation framework [24] and Model Order Reduction [25] to facilitate the numerical implementation of multi-joint systems. At the same time, it is important to replicate a DJ model with human joint geometry to assess joint stresses more accurately. Previous work has already seen the development of FEMs of human finger metacarpophalangeal joints [26]. Adding such models into the DJ-SA, while also incorporating joint cartilage and skin layers should allow for a more comprehensive evaluation of actuator performance. To validate these human-like FEM models it is essential to develop a physical dummy that can mimic the behavior of human finger joints. In this study, we have replicated joint stiffness using a linear torsion spring. Previous studies have however shown that joint stiffness variates nonlinearly depending on the bending angle of the joint [27]. Further studies should be done for developing a physical joint that can mimic this behavior. Furthermore, the CoF values between the Soft Actuator and PLA are different from those between the Soft Actuator and skin, which can affect the performance of the actuator when placed over the joint, future studies, should be done to find materials that can closely approximate the frictional properties of skin. Once our FEM is validated, using these human-like physical dummy joints it could be used for the evaluation of the joint stresses applied from the soft actuator to a patient's joint. Further validation methods of the DJ-SA Complex Model are also necessary, such as considering measurement methods of contact forces without altering the interaction between the DJ and the actuator. Regarding human trials, it is essential to first investigate the adaptation of the DFSA's elongation and bending sections to suit multi-joint

systems and multiple joint sizes. With respect to the design of the DFSA for different joint sizes, in this study, we have proposed 3 criteria (Contact Force-Bending Angle relationship, Blocked Joint-Bending Angle relationship, and tip displacement) that could be used to evaluate the performance of the DFSA and select the adequate sizes for the bending section and elongation section when adapted for different joint sizes. Additionally, in [6] the adequate size of the OMA was shown to be proportional to dummy joint sizes, further studies should be performed on different joint sizes to see if this proportionality can also be applied to the current ratio between elongation section and bending section for the DFSA. Additionally, conducting lifecycle testing in future research is imperative to enhance the DFSA's real-world applicability in rehabilitation settings. Mobile air pump systems should also be developed in order to move the area of soft robotics towards different practical applications such as at-home rehabilitation.

VI. Conclusion

A novel soft actuator, the Dual Function Soft Actuator (DFSA), was proposed and compared to a previous Original Modular Actuator Design (OMA). The DFSA exhibits a superior relationship between input air pressure and bending angle while reducing the contact forces applied to the dummy joint. We also developed and validated a novel FEM of a soft actuator when worn on a dummy joint. This FEM demonstrated the DFSA's more efficiently transform contact force into bending angle when bending the dummy joint. Simulation results also showed that the DFSA has a more efficient force transmission than the OMA when measuring the force applied by the dummy on the blocked joint configuration. By designing an adequately sized elongation section for the DFSA we were also able to reduce how much the actuator slides over the dummy joint.

References

[1] M. Yousufuddin and N. Young, "Aging and ischemic stroke," Aging, vol. 11, no. 9, pp. 2542–2544, 2019. doi:10.18632/aging.101931

[2] J. Wissel, A. Manack, and M. Brainin, "Toward an epidemiology of poststroke spasticity," Neurology, vol. 80, no. Issue 3, Supplement 2, 2013. doi:10.1212/wnl.0b013e3182762448

[3] C.-Y. Chu and R. M. Patterson, "Soft robotic devices for hand rehabilitation and assistance: A narrative review," Journal of NeuroEngineering and Rehabilitation, vol. 15, no. 1, 2018. doi:10.1186/s12984-018-0350-6

[4] Y. Wang et al., "Designing soft pneumatic actuators for thumb movements," IEEE Robotics and Automation Letters, vol. 6, no. 4, pp. 8450–8457, 2021. doi:10.1109/lra.2021.3105799.

[5] T. Tarvainen, J. Fernandez-Vargas, and W. Yu, "New Layouts of Fiber Reinforcements to Enable Full Finger Motion Assist with Pneumatic Multi-Chamber Elastomer Actuators," Actuators, vol. 7, no. 2, p. 31, Jun. 2018, doi:10.3390/act7020031

[6] S. Kokubu et al., "Evaluation of fiber-reinforced modular soft actuators for individualized soft rehabilitation gloves," Actuators, vol. 11, no. 3, p. 84, Mar. 2022. doi:10.3390/act11030084

[7] P. Polygerinos et al., "Soft robotic glove for hand rehabilitation and task specific training," 2015 IEEE International Conference on Robotics and Automation (ICRA), 2015. doi:10.1109/icra.2015.7139597

[8] S.-S. Yun, B. B. Kang, and K.-J. Cho, "Exo-Glove PM: An easily customizable modularized pneumatic assistive glove," IEEE Robotics and Automation Letters, vol. 2, no. 3, pp. 1725–1732, 2017. doi:10.1109/lra.2017.2678545

[9] M. S. Xavier, A. J. Fleming, and Y. K. Yong, "Finite Element Modeling of Soft Fluidic Actuators: Overview and recent developments," Advanced Intelligent Systems, vol. 3, no. 2, 2020. doi:10.1002/aisy.202000187

[10] F. Connolly, C. J. Walsh, and K. Bertoldi, "Automatic design of fiber-reinforced soft actuators for trajectory matching," Proceedings of the National Academy of Sciences, vol. 114, no. 1, pp. 51–56, 2016. doi:10.1073/pnas.1615140114

[11] W. Xiao, D. Hu, W. Chen, G. Yang, and X. Han, "Design, Characterization and Optimization of Multi-directional Bending Pneumatic Artificial Muscles," Journal of Bionic Engineering, vol. 18, no. 6, pp. 1358–1368, Nov. 2021, doi: https://doi.org/10.1007/s42235-021-00077-w.

[12] F. Matsunaga et al., "Finger joint stiffness estimation with joint modular soft actuators for hand telerehabilitation," Robotics, vol. 12, no. 3, p. 83, 2023. doi:10.3390/robotics12030083

[13] J. Zhang, H. Wang, J. Tang, H. Guo and J. Hong, "Modeling and design of a soft pneumatic finger for hand rehabilitation," *2015 IEEE International Conference on Information and Automation*, Lijiang, China, 2015, pp. 2460-2465, doi: 10.1109/ICInfA.2015.7279699.

[14] H. Jeong and W. D. Wang, "Self-adaptive detachable pneumatic soft actuators using uniformly distributed temporary-bonding-fasteners for wearable applications," Sensors and Actuators A: Physical, vol. 349, p. 114083, 2023. doi:10.1016/j.sna.2022.114083

[15] Shota Kokubu, R. Nishimura, and W. Yu, "Deriving Design Rules for Personalization of Soft Rehabilitation Gloves," IEEE Access, pp. 1–1, Jan. 2024, doi: https://doi.org/10.1109/access.2023.3349249.

[16] Human Hand Dimensions Data for Ergonomic Design 2010., Osaka: Research Institute of Human Engineering for Quality Life, 2010.

[17] G. Decroly, B. Mertens, P. Lambert, and A. Delchambre, "Design, characterization and optimization of a soft fluidic actuator for Minimally Invasive Surgery," International Journal of Computer Assisted Radiology and Surgery, vol. 15, no. 2, pp. 333–340, 2019. doi:10.1007/s11548-019-02081-2

[18] D. Maruthavanan, A. Seibel, and J. Schlattmann, "Fluid-structure interaction modelling、of a soft pneumatic actuator," Actuators, vol. 10, no. 7, p. 163, 2021. doi:10.3390/act10070163

[19] P. Zhang, Z. Hu, H. Xie, G.-H. Lee, and C.-H. Lee, "Friction and wear characteristics of polylactic acid (PLA) for 3D printing under reciprocating sliding condition," Industrial Lubrication and Tribology, vol. 72, no. 4, pp. 533–539, 2019. doi:10.1108/ilt-11-2016-0280

[20] O. H. Yeoh, "Some forms of the strain energy function for rubber," Rubber Chemistry and Technology, vol. 66, no. 5, pp. 754–771, 1993. doi:10.5254/1.3538343

[21] L. Labazanova, Z. Wu, Z. Gu, and D. Navarro-Alarcon, "Bio-inspired design of artificial striated muscles composed of sarcomere-like contraction units," 2021 20th International Conference on Advanced Robotics (ICAR), 2021. doi:10.1109/icar53236.2021.9659330

[22] F. Zivic et al., "The influence of the 3D printing infill and printing direction on friction and wear of polylactic acid (PLA) under rotational sliding," Journal of Friction and Wear, vol. 42, no. 2, pp. 106–111, 2021. doi:10.3103/s1068366621020124

[23] C. Tawk and G. Alici, "Finite Element Modeling in the Design Process of 3D Printed Pneumatic Soft Actuators and Sensors," Robotics, vol. 9, no. 3, p. 52, Jul. 2020, doi: https://doi.org/10.3390/robotics903005

[24] E. Coevoet et al., "Software toolkit for modeling, simulation, and control of Soft Robots," Advanced Robotics, vol. 31, no. 22, pp. 1208–1224, 2017. doi:10.1080/01691864.2017.1395362

[25] S. M. H. Sadati, S. Naghibi, L. da Cruz, and C. Bergeles, "Reduced order modeling and model order reduction for Continuum manipulators: An overview," Frontiers in Robotics and AI, vol. 10, 2023. doi:10.3389/frobt.2023.1094114

[26] K. Butz, G. Merrell, and E. Nauman, "A three-dimensional finite element analysis of finger joint stresses in the MCP joint while performing common tasks," HAND, vol. 7, no. 3, pp. 341–345, 2012. doi:10.1007/s11552-012-9430-4

[27] X. Q. Shi, H. L. Heung, Z. Q. Tang, K. Y. Tong, and Z. Li, "Verification of Finger Joint Stiffness Estimation Method With Soft Robotic Actuator," Frontiers in Bioengineering and Biotechnology, vol. 8, Dec. 2020, doi: 10.3389/fbioe.2020.592637